Journal of Catalysis 260 (2008) 103–112

Contents lists available at ScienceDirect

Journal of Catalysis

www.elsevier.com/locate/jcat

Catalyst size matters: Tuning the molecular mechanism of the water–gas shift reaction on titanium carbide based compounds

Francesc Viñes [a], Jose A. Rodriguez [b], Ping Liu [a], Francesc Illas [a,*]

[a] Departament de Química Física & Institut de Química Teòrica i Computacional (IQTCUB), Universitat de Barcelona, C/Martí i Franquès 1, 08028 Barcelona, Spain
[b] Chemistry Department, Brookhaven National Laboratory, Upton, New York, NY 11973, USA

ARTICLE INFO

Article history:
Received 11 July 2008
Revised 10 September 2008
Accepted 11 September 2008
Available online 14 October 2008

Keywords:
Water–gas shift reactions
TiC
H_2 production
Density functional calculations

ABSTRACT

The molecular mechanism of the water–gas shift reaction catalyzed by titanium carbide compounds was studied using a density functional approach. Three different catalyst models have been considered: the extended TiC(001) surface, the Ti_8C_{12} MetCar, and a $Ti_{14}C_{13}$ nanoparticle. Adsorption of reactants, intermediates, and products occurs on different sites, demonstrating the chemical versatility of the TiC substrates. Thus, adsorption energies depend not only on the existence of low-coordinated sites, but also on the nature of atoms involved in the adsorption site. The two most likely molecular mechanisms, redox and associative, were considered. The first of these mechanisms involves complete water dissociation, whereas the second involves formation of the carboxyl (OCOH) intermediate. The catalytic activity was found to be highest for the TiC(001) surface, due to the overly strong adsorption of reactants and products on either $Ti_{14}C_{13}$ or Ti_8C_{12}. This has important consequences for the underlying chemistry, as evidenced by the corresponding reaction energy profiles, which show that the redox mechanism is the preferred route for the reaction occurring on the nanoparticles, whereas the carboxyl formation route is preferred for the reaction occurring above the TiC(001) surface. However, the calculated reaction rate constants indicate that the reaction will hardly occur on the former, whereas it is quite feasible on the latter. The present study suggests that TiC and similar transition metal carbides can be good catalysts for the water–gas shift reaction and can be potential substitutes for current low-temperature catalysts. In addition, the results point to a possible tuning to control the particle size or rate of steps.

1. Introduction

Generation of pure H_2 streams has become quite important in the last decade, not only because of its use in the chemical industry [1–3], but also because modern hydrogen-based fuel cells appear to be one of the most promising environmentally friendly substitute for gas–oil and biodiesel vehicle fuels [4]. Today, nearly 95% of the H_2 used in industry is generated essentially from hydrocarbons [5]. As a result, the final streams can contain up to 10% of CO [6], which can strongly bind on the Pt electrode surface, eventually poisoning and degrading the fuel cell performance. In this sense, the water–gas shift (WGS) reaction ($CO + H_2O \rightarrow H_2 + CO_2$) constitutes a critical process for on-board generation and purification of H_2. Consequently, a hydrogen fuel economy requires improved air-tolerant [7,8], cost-effective WGS catalysts for lower-temperature processing [9,10] allowing mobile fuel cell applications under cyclic and stationary conditions [2]. Current industrial catalysts consisting of mixtures of Fe–Cr and Zn–Al–Cu oxides catalyze the WGS reaction at temperatures between 350–500 and 180–250 °C, respectively [11,12]; however, these catalysts are pyrophoric [8] and normally require lengthy and complex activation steps before use. Consequently, alternative catalysts are being sought [1,2,5,10].

In the past few years, many experimental and theoretical studies have addressed the search for potential WGS reaction catalysts to replace the commercial ones [13]. For instance, several problems can be solved using Pt, Cu, or Au nanoparticles [14–17] supported on reducible oxides (TiO_2, ZnO, and especially CeO_2). The simultaneous presence of the support and the metal nanoparticle is crucial, because the supports do not catalyze the WGS reaction, and the metal extended surfaces do not present high reactivity [8,9]. In fact, the high activity appears to be inherent to the use of supported nanoparticles, with the best performance achieved when using a 1%–10% noble-metal weight ratio [18,19]. Despite this fact, however, the WGS reaction molecular mechanism and the role of the different sites remain obscure and the subjects of much discussion [9,14–17,20–22]. The importance of the substrate has been highlighted only very recently, with compelling evidence that the support is not a mere reaction spectator, but instead directly participates in the reaction. For instance, the high reactivity observed when using CeO_2 as a support [8,9,23,24] arises from the fact that

* Corresponding author.
E-mail address: francesc.illas@ub.edu (F. Illas).

0021-9517/$ – see front matter
doi:10.1016/j.jcat.2008.09.011

CeO_2 surface oxygen vacancies can readily dissociate H_2O, which indeed constitutes the rate-limiting step (RDS) on both the current catalysts and on noble metals [25]. Nevertheless, the evident economic costs of the use of noble metals, along with the fact that CO accumulation on the metal nanoparticles can deactivate the catalyst after long use, prevent the wide use of such metal-supported catalysts in the WGS reaction [26,27].

One class of materials that are stable, low cost, and not poisoned by CO is the early transition-metal carbides (TMCs). TMCs have been cited as potential substitutes for precious metal catalysts in a wide variety of reactions because of the similar, sometimes better, catalytic behavior compared with noble metals [28–30]. It has already been noted that although the catalytic activity of TMCs is close to that exhibited by noble metals, the kinetics and, more importantly, product selectivities are often different, suggesting that these materials may provide unique catalytic pathways [30]. Recent experiments have indeed found that TMCs are attractive candidates for replacing Cu-based catalysts in fuel cell-powered automotive vehicles because they demonstrate greater activity and stability during the WGS reaction [31,32]. Nevertheless, the use of TMCs as catalysts for the WGS reaction faces problems, because oxycarbide species can be formed under reaction conditions [29–33]. Solving these problems requires an intimate knowledge of the underlying WGS molecular mechanism, which has remained elusive. The main objective of the present study is to provide theoretical information on the feasibility of the WGS reaction catalyzed by TMC and to unravel the molecular details of the reaction mechanism.

It is known that the chemical activity of TMC depends strongly on the metal/carbon ratio and on the size of the system [34,35]. Ensemble and electronic effects lead to a moderate chemical reactivity for TMC(001) surfaces (TM = Ti, V, Zr, Nb, Mo, Hf, Ta, and W) [36]. In these systems, a metal → carbon electron transfer, evidenced experimentally [37], and subsequent stabilization of the metal *d* band produce metal sites with a relatively low reactivity. On the other hand, the C sites in the surface can be chemically active and bind species like O and S [38–40]. Furthermore, stable TMC nanoparticles, such as the MetCar [41] (TM_8C_{12}) or the nanocrystal [42] ($TM_{14}C_{13}$), can exhibit different, unique activity compared with transition metal (TM) surfaces and $TM_2C(001)$ or TMC(001) transition metal carbide surfaces [34,43–45]. For some chemical reactions, these TMC nanoparticles are very active despite their high or low carbon concentrations, whereas in other cases they are surprisingly inert. This unexpected activity pattern results from interplay of shifts in the metal d-bands and distortions in the geometry of the metal carbide nanoparticles [40].

Previous density functional (DF) calculations coupled to a microkinetic model concerning the WGS reaction on $Mo_2C(001)$ surfaces have been reported [33,46]. The DF results showed that the WGS reaction follows a redox mechanism in which successive oxidation and reduction of the surface occurs, in contrast with the associative mechanism followed on Cu(111)—the main component of the WGS reaction commercial catalysts [11]—also recently evidenced by DF calculations [47]. In any case, despite the similar electronic structure of $Mo_2C(001)$ and Pt(111) surfaces, as evidenced by the d-band structure and d-band center [48], Mo_2C exhibits low activity, due to the fact that both Mo and C sites bond oxygen too strongly to allow its facile removal and lead to O-poisoning [33]. Only the C-Mo_2C covered by oxygen displays a similar WGS activity to that of the current catalysts, although eventual carbon removal would decimate the high catalytic activity. The formation of oxycarbide species can be avoided by using a less active TMC than Mo_2C. In principle, TiC(001) seems to be a good candidate, because it does not bind O as strongly as $Mo_2C(001)$ and does not bind CO as strongly as Pt(111). Due to ensemble and electronic effects induced by carbon, TiC(001) exhibits a lower reactivity toward adsorption of different species compared with that reported for $Mo_2C(001)$ [49–51]. For instance, the calculated adsorption energy of CO on TiC(001) of 0.36 eV is much smaller that the value of 2.35 eV reported for CO on the $Mo_2C(001)$ and the interaction of other probe molecules such as H_2O or NH_3 is also rather weak (0.47 eV and 0.27 eV, respectively) [49]. In addition, the experimental adsorption energy of CO on TiC(001) is only 0.46 eV, lower than that on Pt(111) [51]. Furthermore, TiC(001) is less reactive and more stable than other titanium carbide surfaces, such as TiC(111) [47].

Herein we provide compelling evidence of the different catalytic activities of the titanium carbide (001) surface and of its nanoparticles, MetCar (Ti_8C_{12}) and the nanocrystal ($Ti_{14}C_{13}$)—through exhaustive and systematic exploration of the corresponding potential energy surface by means of DF calculations. We found that the size of the TiC underlying substrate controls the molecular mechanism. If fact, on TiC(001), the WGS reaction follows an associative mechanism, involving the formation of a carboxyl (OCOH) species, similar to that on the Cu(111) surface [47], whereas when the reaction is mediated by the $Ti_{14}C_{13}$ nanocrystal or Ti_8C_{12} MetCar, the reaction undergoes a redox mechanism, involving the complete dissociation of water. Moreover, the TiC(001) surface catalyzes the reaction, a achieving sufficiently fast reaction rate. Finally, we found that despite of the Pt-like behavior of TMC, its use in the form of nanoparticles is not favorable in catalysis, either because it could lead to the eventual formation of an inactive oxycarbide or because the reaction rate will decrease significantly.

2. Computational details, cluster and surface models

The present study is based on periodic DF calculations carried out within the usual Kohn–Sham implementation and using the PW91 form of the generalized gradient approximation (GGA) for the exchange-correlation potential [52]. A plane-wave basis set was used, with the kinetic energy cutoff set to 415 eV. The effect of the atomic cores on valence density was taken into account by means of the projector-augmented wave (PAW) method of Blöchl [53]. A conjugated gradient algorithm was used for the convergence of geometrical parameters, with a total energy threshold of 0.001 eV. In all cases, this ensures forces <0.03 eV/Å. Non-spin-polarized calculations were carried out unless stated otherwise. A Gaussian smearing with a 0.2 eV width was used to improve the convergence, although the final energies were always extrapolated to 0 K. All calculations were carried out using the VASP 4.6 code [54–56].

A slab model was used to represent the TiC(001) surface. As expected, this was found to be the most stable crystal face for the *fcc* crystal packing of TiC and other TMCs. It has the same number of Ti and C atoms and displays significant rumpling, with the C atoms displaced outward toward the vacuum while the Ti atoms relax inward [36]. A $(\sqrt{2} \times \sqrt{2})45^\circ$ unit cell repeated periodically with a vacuum region of 10 Å between the repeated slabs was used to represent the TiC(001) surface (Fig. 1a). The slab model was constructed using the lattice parameter optimized for the bulk, as reported previously [36]. The slab contains four atomic layers, the two outermost of which were allowed to relax completely. An optimum Monkhorst–Pack grid of $13 \times 13 \times 1$ was used to select the special *k*-points needed to carry out numerical integrations in the reciprocal space of the TiC(001) unit cell described above, as reported previously [36].

The discrete $Ti_{14}C_{13}$ and Ti_8C_{12} systems (Figs. 1b and 1c) were modeled, placing them inside a $15 \times 15 \times 15$ Å cubic cell, which guarantees a minimum separation of 10 Å between the repeated images and consequently a negligible interaction between them. This strategy provides accurate results without increasing the basis set cutoff and has been proven valid for studying reactivity on

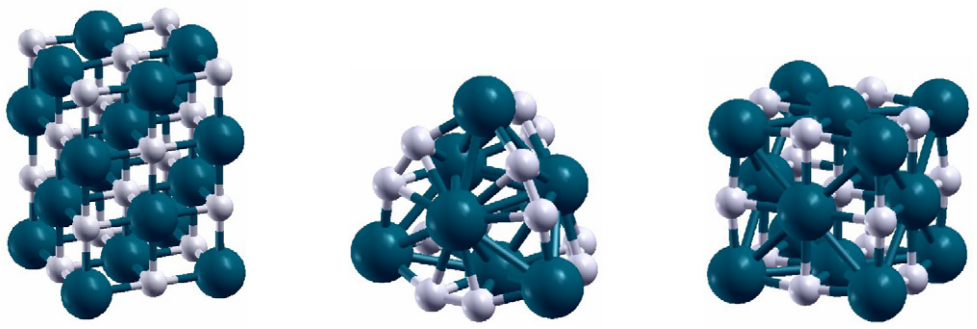

(a) (b) (c)

Fig. 1. Optimized structures of (a) TiC(001) surface unit cell, (b) Ti_8C_{12} MetCar nanoparticle and (c) the $Ti_{14}C_{13}$ nanocrystal. Big blue and small white spheres represent Ti and C atoms, respectively. (For interpretation of the references to color in this figure legend, the reader is referred to the web version of this article.)

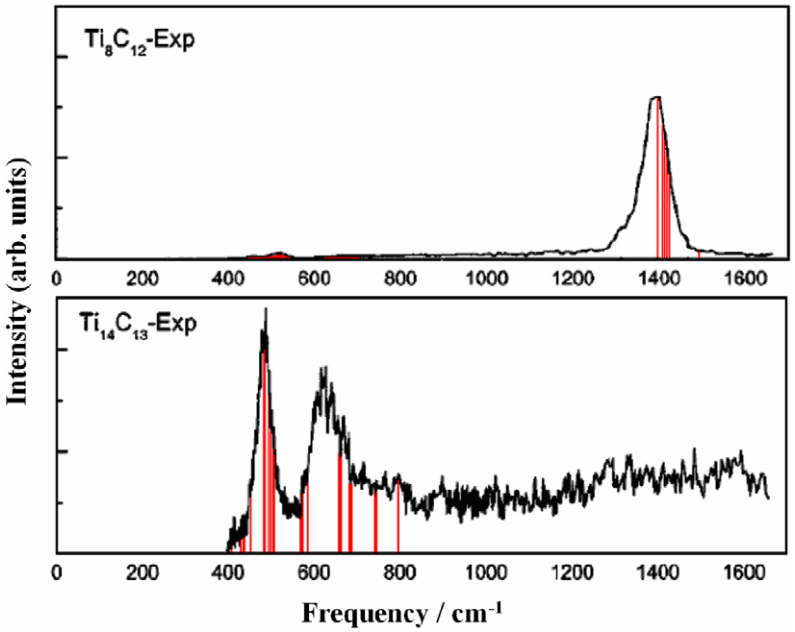

Fig. 2. Experimental spectra [65] of Ti_8C_{12} MetCar (upper panel) and $Ti_{14}C_{13}$ nanocrystal (lower panel). Positions of calculated vibrational frequencies are denoted in red lines. Note that theoretical intensities have been added as a guide to the eyes. (For interpretation of the references to color in this figure legend, the reader is referred to the web version of this article.)

isolated nanoparticles [57–59]. The atomic positions of all atoms in the $Ti_{14}C_{13}$ nanocrystal and Ti_8C_{12} MetCar were allowed to relax fully during geometry optimization calculations with no constraints. Because these are discrete systems, calculations were carried out at the Γ point. Optimization of isolated reaction species was done in a similar way, but using a broken symmetry cell of $14 \times 15 \times 16$ Å to get a correct molecular orbital occupation. Spin-polarized calculations were performed for open-shell species.

A slightly distorted tetrahedral shape was chosen for Ti_8C_{12} MetCar, because this was found to be the most stable shape by previous experimental [60,61] and theoretical studies [34,62–64]. This structure (Fig. 1b) implies Ti atoms at the corners (hereafter designated titanium-outside [Ti^o]) and at the center of the facets (titanium inside [Ti^i]), whereas C_2 groups are located at the tetrahedral edges. The $Ti_{14}C_{13}$ nanocrystal exhibits a cubic shape, with Ti atoms at the corners (Ti^o), and at the centers of the facets (Ti^i); C atoms are located at the nanoparticle edges. In fact, the nanocrystal could be viewed as a bulk cubic section and used as a model to study reactivity on the steps of the TiC(001) surface. Spin-unrestricted calculations for both systems converge to a closed shell electronic structure, in line with previous calculations [34,63,64]. For these two discrete systems, harmonic vibrational frequencies were calculated for the optimized isolated structures, through evaluation of the forces on each nucleus in the three spatial coordinates using a finite difference scheme, displacing the atoms by 0.05 Å. Fig. 2 shows that the position of the calculated frequencies agree quite well with the experimental infrared (IR) spectra [65], also in line with previous calculations [66,67].

Transition states (TS) of different reaction elementary steps were located using the climbing-image nudged elastic band [68,69] (CI-NEB) method, as implemented in the VASP [54–56] code. The TS structures thus found were refined by subsequent quasi-Newton relaxation of the highest CI-NEB image, using a force threshold of 0.03 eV/Å and allowing both the adsorbed species and the substrate to relax as described above. Stationary points fulfilling the force criteria defined above were further characterized as TS through pertinent vibrational frequency analysis. The same frequency analysis also was carried out to characterize reactants and products as minima in the potential energy surface. Note that translational and rotational modes were taken into account, because their movement is frustrated by the substrate, and thus they become true vibrational modes. This TS search procedure has proven to give proper energy barrier results when studying reactions on carbides [70,71].

For the elementary reaction steps of interest, the rate constant was estimated through the transition state theory, using the calculated vibrational frequencies of reactants and TS species to estimate the entropy contribution to the free energy variation in terms of vibrational partition functions [72]. Thus,

$$k = \left(\frac{k_B T}{h}\right)\left(\frac{q^{\#}}{q}\right) e^{-E_{barr}/k_B T}, \quad (1)$$

where k is the reaction rate constant of the studied step, k_B is the Boltzmann constant, T is the temperature in K, $q^{\#}$ and q are the vibrational partition functions for the TS and initial state, respectively, and E_{barr} is the activation energy of the elementary step corrected to the zero point energy, adding the first vibrational energy level of every real normal vibration mode. Note, however, that reaction rates depend not only on thermodynamics and preexponential factors, but also on coverage of different species during the reaction. Comparing calculated rate constants provides useful insights into the reaction processes, although it is worth pointing out that a detailed description of the entire process reaction under working conditions requires a microkinetic modeling including *all* possible reaction steps [33,47,73].

3. Water–gas shift reaction elementary steps

Two main mechanisms have been proposed for the WGS reaction. The first is the regenerative redox mechanism [74–76], which involves successive oxidation and reduction of the substrate and can be decomposed in the following elementary steps:

$$H_2O + * \leftrightarrow H_2O^*, \quad (1)$$

$$CO + * \leftrightarrow CO^*, \quad (2)$$

$$H_2O^* + * \leftrightarrow OH^* + H^*, \quad (3)$$

$$OH^* + * \leftrightarrow O^* + H^*, \quad (4)$$

$$CO^* + O^* \leftrightarrow CO_2^*, \quad (5)$$

$$H^* + H^* \leftrightarrow H_2^* + *, \quad (6)$$

$$CO_2^* \leftrightarrow CO_2 + *, \quad (7)$$

and

$$H_2^* \leftrightarrow H_2 + *, \quad (8)$$

where $*$ represents an available adsorption site. A second, associative mechanism has been found to be crucial when the WGS reaction occurs on noble metals and on commercial catalysts [18,19,25,47,77,78]. The importance of this alternative pathway for the WGS reaction on Mo_2C was clearly demonstrated by Liu and Rodriguez [33], who pointed out the similarity between the chemistry of TMC and of the Pt group metals [28,36]. In this mechanism, a carboxyl intermediate is formed that eventually decomposes on carbon dioxide and atomic hydrogen, thereby avoiding the formation of surface atomic oxygen. The following elementary steps would replace steps (4) and (5):

$$CO^* + OH^* \leftrightarrow OCOH^{**} \quad (9)$$

and

$$OCOH^{**} \leftrightarrow H^* + CO_2^*. \quad (10)$$

Finally, is worth mentioning that the OH disproportionation step,

$$OH^* + OH^* \leftrightarrow H_2O^* + O^*, \quad (11)$$

has been found to be a fast step for the WGS reaction on Pt(111), thus providing an alternative route for atomic oxygen generation [73]. The origin of the efficiency for this step is the rather short distance between neighboring adsorbed OH* species (2.76 Å), which favors a rather strong interaction between the adsorbed species (0.45 eV), with a concomitant decrease of the energy barrier with respect to the case in which the OH* groups are far from each other. In the case of the TiC(001) surface, the distance between OH* neighbors is on the order of 3.0 Å, with a concomitant decrease in their interaction (0.04 eV). Thus, the proximity of the two OH groups does not contribute to decrease the energy barrier, which will be as shown in step (4). Consequently, step (11) was not considered further.

It is worth mentioning that long-term reaction rates on TiC-based compounds can depend critically on the molecular mechanism followed. We already mentioned that both theoretical calculations [33,38] and experiments [79] have shown that surface atomic oxygen binds strongly to TMC, eventually leading to oxycarbide formation, specially at temperatures above 500 K and at 300 K at surface step edges [80]. Although the oxycarbide formation of TiC is exothermic, previous theoretical calculations have shown that the initial step involves an endothermic process with a barrier above 0.6 eV. But two or more oxygen atoms can act cooperatively, avoiding this initial energy barrier [81]. Thus, the catalyst can be degraded in the presence of a certain amount of oxygen. In this sense, comparing the reaction rates for steps (4) and (9) can provide important information about the molecular mechanism followed by the WGS reaction under certain conditions. Toward this end, TSs were located and reaction rates estimated for both reaction steps on all three substrates as possible mechanism-determining steps (MDSs), in contrast to the RDSs. Finally, reaction step (3) also was studied on all of the systems, because it represents the RDS on the catalysts studied previously [9,18,19]. The TSs for reaction steps (5), (6), and (10) were located for completeness for the reaction on the extended TiC(001) surface, which, as we show below, is the only substrate that can effectively catalyze this reaction.

In any case, it must be kept in mind that in the present work we did not exhaustively examine all possible reaction steps implied in the reaction. In fact, the aim of the present study is to compare simple steps of the most likely mechanisms and to reveal suitability of TMC as catalyst, rather than to study all possible steps in depth on every system.

4. Adsorption landscapes of reaction species

All possible adsorption sites of WGS reaction reactants (H_2O and CO), products (H_2 and CO_2), and intermediates (OH, H, O, and OCOH) on the TiC(001) extended surface, on the $Ti_{14}C_{13}$ nanocrystal, and on the Ti_8C_{12} MetCar were systematically explored. These included mono-, bi- and tri-coordinated adsorption sites and all combinations of interactions between the atoms of the adsorbate and the substrate. Fig. 3 shows the most stable adsorption site of every species on every substrate, together with the calculated adsorption energy, E_{ads}^{A}, defined as

$$E_{ads}^{A} = E_{A/B} - (E_A + E_B), \quad (1)$$

where E_{ads}^{A} is the adsorption energy of species A, $E_{A/B}$ is the energy of the system containing the A adsorbed on the substrate B, E_A is the energy of gas phase A at its corresponding relaxed geometry, and E_B is the energy of the previously optimized pristine surface or bare cluster substrate. In all cases, only one atom/molecule was placed on the surface of the corresponding model system. Spin-polarized test calculations carried out for each case revealed no significant changes in either the adsorption energy or the energy level occupations. These findings are in line with those of previous DF studies of the adsorption of H_2, H_2O, and CO on MetCar and nanocrystal particles [67,82,83].

At first glance, the results seem to show that both $Ti_{14}C_{13}$ and Ti_8C_{12} nanoparticles are more active compared with the ex-

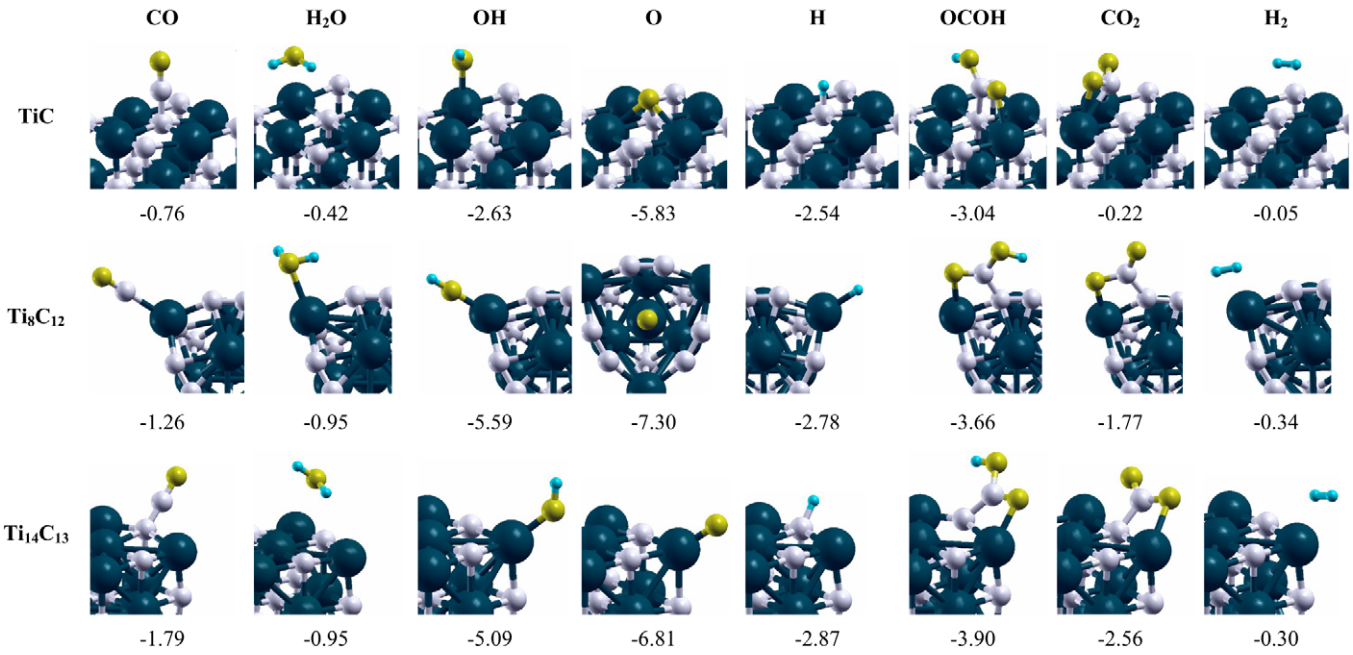

Fig. 3. Most stable adsorption sites, optimized adsorbate structures and corresponding adsorption energies (in eV) for the WGS reaction products, intermediates and reactants on TiC(001), Ti_8C_{12} and $Ti_{14}C_{13}$. Big blue and small white spheres represent Ti and C atoms, respectively, while small light blue and yellow spheres correspond to H and O atoms, respectively. (For interpretation of the references to color in this figure legend, the reader is referred to the web version of this article.)

tended TiC(001) surface. This is due simply to the existence of low-coordinated atoms in these nanoparticles, which enhances their reactivity [67]. This would be particularly true for the Ti^o sites, because these are the less coordinated ones. This statement cannot be used as a rule of thumb, however. In fact, the adsorption energy depends not only on the coordination between the adsorbate and the substrate, but also on the chemical nature of the atoms involved in the chemical bond and on its chemical nature. Thus, Ti^o is not always the most favorable adsorption site. In fact, CO and H are more strongly bonded to substrate carbon atoms on the nanocrystal and on the TiC(001) surface, and, surprisingly, Ti^i is the most stable site for atomic oxygen on MetCar. This latter finding reveals a quite strange behavior in terms of lower-coordination/higher-activity arguments. In fact, despite the report by Liu et al. [67] indicating a special reactivity for this particular site on MetCar compared with similar sites on either the $Ti_{14}C_{13}$ nanocrystal or the TiC(001) surface, as far as we know, this is the first reported case in which Ti^i was found to be the most stable site. Finally, important H ↔ C or C ↔ C interactions with the substrate carbon sites occur, increasing the stability of adsorbed CO_2, H_2O, and OCOH species.

In addition, these species are not always more strongly bonded on MetCar, as would expected due to the fact that this is the system with the lowest coordination. In fact, OH and O are more strongly bonded to MetCar, while CO, CO_2 and OCOH are more strongly bonded to the nanocrystal. H_2O, H_2 and H species present similar adsorption energy values for the MetCar and the nanoparticle. We can state that in general, species binding through an oxygen atom are more strongly bonded on MetCar, whereas species binding through a carbon atom are more strongly bonded on the nanocrystal. Finally, species with high quantity of hydrogen adsorb indistinctly on either MetCar or the nanocrystal. Here is important to point out that the overall adsorption energies of the different species are rather high for both MetCar and the nanocrystal, and that, according to Sabatier's principle [84], high adsorption energies necessarily imply large energy barriers and low reaction rates, indicating that these systems are poor catalysts. However, the adsorption energies on the extended TiC(001) surface are rather low for both reactants and products and moderate for reaction intermediates, pointing to better catalytic activity. Indeed, in experiments performed at Brookhaven National Laboratory and the Tokyo Institute of Technology [85], TiC(001) and extended surfaces of titanium carbide were found to be much more active and stable WGS catalysts than TiC_x ($x = 0.8$–1.3) nanoparticles dispersed on an inert Au(111) substrate. The performance and WGS reaction rates on MetCar, $Ti_{14}C_{13}$ nanocrystal, and TiC(001) surface are discussed in more detail in the next section.

5. Reaction mechanism on MetCar and nanocrystal

The adsorption landscapes discussed in the previous section allow us to investigate the feasibility of the WGS reaction on the MetCar and nanocrystal supports. The TSs corresponding to reaction elementary steps (3), (4), and (9), hereinafter refereed as TS^1, TS^2, and TS^3, respectively, were located as described previously. Several sensible reaction pathways were examined for each reaction step. These reaction pathways included not only the direct reaction connecting both reactants and products adsorbed on the most stable sites (depicted in Fig. 3), but also the diffusion of one or more species to less stable adsorption sites. Therefore, the diffusion energy was added to the energy barrier for the corresponding direct path to obtain an effective barrier. We comment only on those pathways with the lowest effective barriers, because they outline the minimum energy pathway (see also Ref. [86]).

Despite calculations revealing that WGS reaction is exothermic by −0.71 eV, in line with previous DF calculations [19,25,47], the gas-phase reaction TS is located 3.75 eV above the reactant energy level. This indicates that the reaction, despite being ther-

Table 1
Zero point corrected energy barriers, E_{barr}, for the water dissociation (TS^1), OH dissociation (TS^2) and carboxyl formation (TS^3) on Ti_8C_{12} MetCar and $Ti_{14}C_{13}$ nanocrystal.

	E_{barr} (TS^1)	E_{barr} (TS^2)	E_{barr} (TS^3)
Ti_8C_{12}	∼0	1.56	1.82
$Ti_{14}C_{13}$	∼0	1.05	1.53

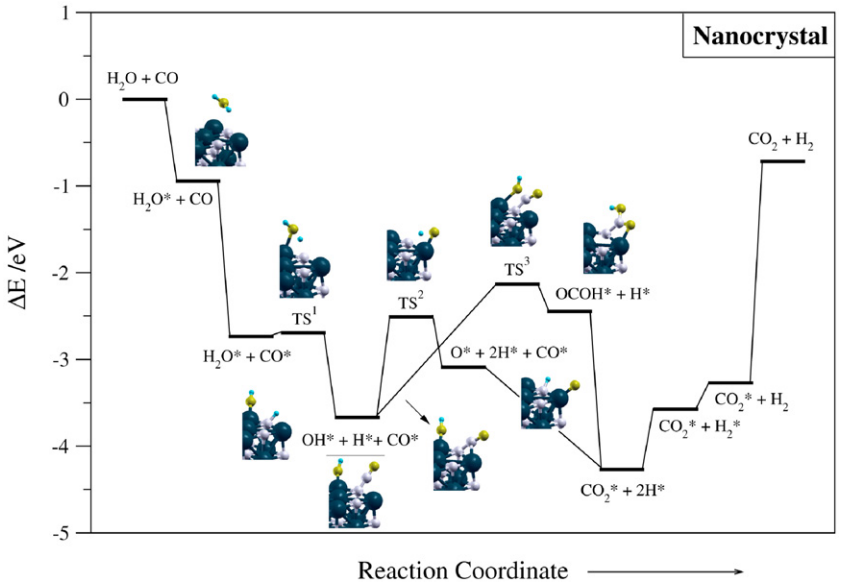

Fig. 4. Calculated energy profile for the WGS reaction on the $Ti_{13}C_{14}$ nanocrystal. All energies have been referred to the non-interacting reactants in gas phase. Big blue and small white spheres represent Ti and C atoms, respectively, while small light blue and yellow spheres correspond to H and O atoms, respectively. (For interpretation of the references to color in this figure legend, the reader is referred to the web version of this article.)

Table 2
Reaction step rate constants, k (in s^{-1}), calculated at 300 K, for the water dissociation (TS^1), OH dissociation (TS^2), and carboxyl formation (TS^3) on Ti_8C_{12} MetCar and $Ti_{14}C_{13}$ nanocrystal.

	k (TS^1)	k (TS^2)	k (TS^3)
Ti_8C_{12}	5.24×10^{13}	1.45×10^{-13}	1.66×10^{-21}
$Ti_{14}C_{13}$	2.02×10^{15}	1.06×10^{-4}	3.29×10^{-14}

modynamically favorable, it is kinetically hindered. Table 1 shows the zero-point-corrected energy barriers of the minimum energy pathways for steps (3), (4), and (9). Here it is worth pointing out that the barriers corresponding to TS^1 were quite small and literally vanished when corrected to include the zero-point energy. This interesting result means that both MetCar and nanocrystal can readily dissociate H_2O, a step that is the RDS on commercial and metal catalysts [9,18,19]. But the energy barriers corresponding to TS^2 and TS^3 were high, and these steps could act as the RDS as well. These high barrier values were due largely to the strong adsorption of the reaction species.

The WGS reaction energy profile catalyzed by the nanocrystal is presented in Fig. 4. Both CO and H_2O are strongly adsorbed on this substrate. After adsorption, H_2O easily dissociates into OH and H, the latter moving to adsorb on a nearby substrate carbon site. OH can dissociate subsequently in a similar way. Carboxyl formation would imply that CO adopted a special conformation (0.13 eV above in energy) in response to an attack by the OH group, eventually leading to the carboxyl species. The reaction rate constants at 300 K were calculated for each step and are listed in Table 2. According to these values, water dissociation occurred very rapidly, whereas the remaining steps were rather slow. In fact, on the nanocrystal—and, by extrapolation, on TiC(001) steps as well—the reaction underwent a redox mechanism, because the rate constant for OH dissociation was 10 orders of magnitude larger than the corresponding rate constant for carboxyl formation. But despite the fact that reaction rates were several orders of magnitude larger than the gas-phase reaction (estimated as 3.14×10^{-34}), they were still too small. In addition, some intermediate states exhibited energies well below those of the reactants and products, indicating that the reaction eventually could be stopped by trapping at these intermediate states.

Similar results were obtained for the reaction catalyzed by the MetCar, as can be readily seen in the reaction profile in Fig. 5. H_2O was rapidly dissociated after adsorption, and H atoms occupied first-neighbor carbon sites, although this was followed by diffusion to Ti^o sites, the preferred sites in this system. Dissociation of OH was similar to that of H_2O, and O also diffused to the most favorable Ti_i site. Carboxyl formation implies CO diffusion to a meta-stable site of 0.21 eV greater energy, from which an OH attack would lead to OCOH. The estimated rate constants suggest a rapid water dissociation step and a quite slow redox mechanism. Thus, despite the fact that the energy barriers for steps (4) and (9) were more similar than those found for the reaction occurring on the nanocrystal, the OH dissociation step was still estimated to be eight orders of magnitude faster than carboxyl formation. In addition, some intermediate states were well below the energy levels of the reactants and products, pointing to possible catalyst poisoning.

6. Reaction mechanism on the TiC(001) surface

The extended TiC(001) surface exhibited much lower activity toward the adsorption of species, as noted in Section 2. This is in contrast with the general trend exhibited by noble metal nanoparticles, which usually exhibit greater adsorption energy than the corresponding extended surfaces. In the case of TiC, adsorption on the extended surface is sufficiently great, and the use of nanoparticles would lead only to stronger adsorption and lower reaction rates and eventually, as we show, to a change in the reaction mechanism.

Because all reaction species are moderately bound to TiC(001), the TSs for all of the reaction steps discussed herein were located and characterized as described above. The transition states for the lowest energy pathways corresponded to carbon dioxide formation as in reaction step (5) and to molecular hydrogen formation and carboxyl decomposition as in reaction steps (6) and (10). Hereinafter, these TSs are designated TS^4, TS^6, and TS^5. Zero-point-corrected energy barriers and estimates of the reaction step rate constants are reported in Table 3, and the WGS reaction energy profile catalyzed by TiC(100) is displayed in Fig. 6. The first reaction steps resemble those described for the reaction on the nanocrystal. In fact, water dissociates in a very sim-

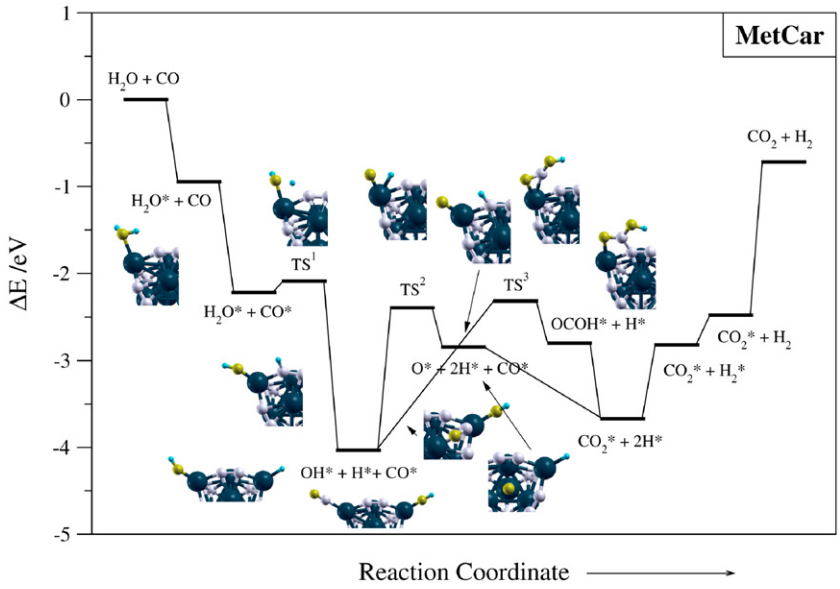

Fig. 5. Calculated energy profile for the WGS reaction on the Ti_8C_{12} MetCar. All energies have been referred to the non-interacting reactants in gas phase. Big blue and small white spheres represent Ti and C atoms, respectively, while small light blue and yellow spheres correspond to H and O atoms, respectively. (For interpretation of the references to color in this figure legend, the reader is referred to the web version of this article.)

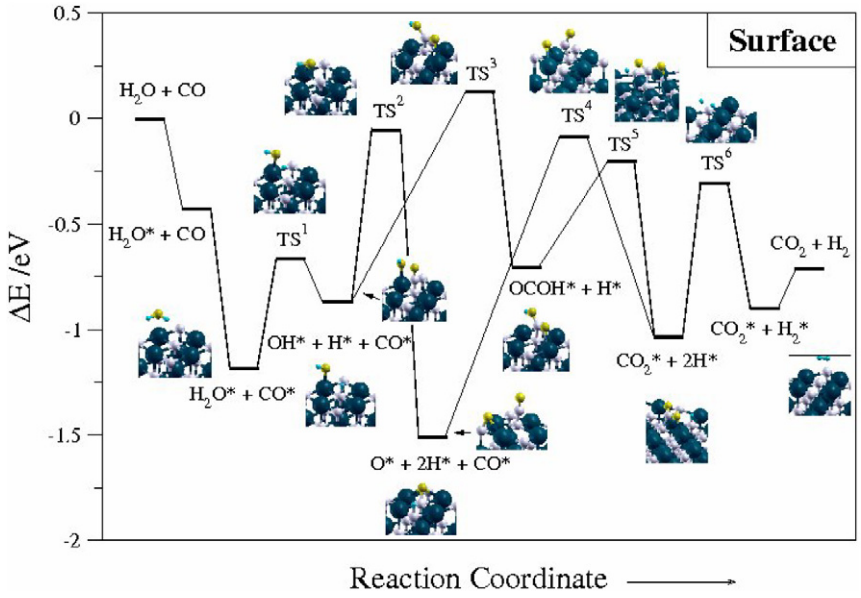

Fig. 6. Calculated energy profile for the WGS reaction energy profile on the TiC(001) extended surface All energies have been referred to the non-interacting reactants in gas phase. Big blue and small white spheres represent Ti and C atoms, respectively, while small light blue and yellow spheres correspond to H and O atoms, respectively. (For interpretation of the references to color in this figure legend, the reader is referred to the web version of this article.)

Table 3
Zero point energy barriers (in eV) and corresponding calculated rate constants (in s^{-1}) at 300 K for the water dissociation (TS^1), OH dissociation (TS^2), carboxyl formation (TS^3), carbon dioxide formation (TS^4), carboxyl decomposition (TS^5), and molecular hydrogen formation (TS^6) on TiC(001) extended surface.

	E_{barr}	k
TS^1	0.37	3.78×10^{8}
TS^2	0.87	2.84×10^{-2}
TS^3	0.88	3.20×10^{0}
TS^4	1.38	9.50×10^{-11}
TS^5	0.36	2.38×10^{8}
TS^6	0.61	1.00×10^{4}

ilar way, although with a significantly higher barrier. But the barrier is still small enough to enable rapid water dissociation, with a rate constant of the order of 10^8 s^{-1}. In contrast to other catalysts [9,18,19], water dissociation on the TiC(001) surface is not the RDS. The next steps are crucial, because they constitute the MDS. The calculated zero-point-corrected energy barriers are essentially the same, although the corresponding rate constants differ significantly. In fact, in principle, carboxyl formation, and thus the associative mechanism, is predicted to be 130 times faster than hydroxyl dissociation, which would lead to the redox mechanism. This is one of the main outcomes of the present work; it clearly demonstrates that the reaction would proceed via a mechanism that avoids the eventual oxidation and degradation of the metal carbide. Thus, the carbon dioxide formation step appears to be irrelevant, despite the fact that it could be considered the redox mechanism RDS due to the high energy barrier and the rather small rate constant.

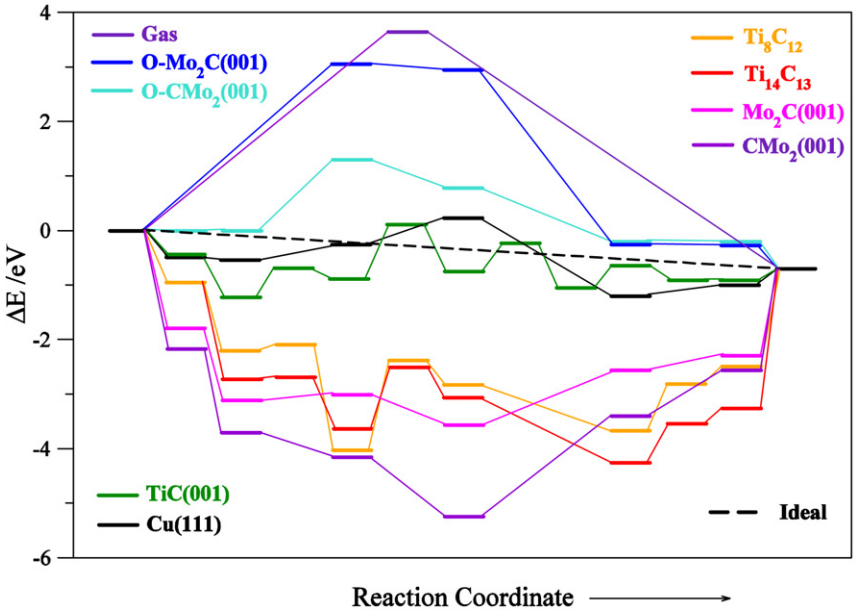

Fig. 7. Comparison of the calculated energy profiles for the WGS reaction on (non-)oxygen-covered Mo_2C surfaces [34], Cu(111) [47], Ti_8C_{12} MetCar, $Ti_{14}C_{13}$ nanocrystal, TiC(001) surface and on gas-phase. Dashed lines would represent the ideal catalyst without activation energies. Only the most favorable pathway is show.

Focusing on the associative mechanism, carboxyl decomposition and molecular hydrogen formation exhibited lower energy barriers and larger rate constants than those of the carboxyl formation step. Thus, the carboxyl formation indeed appears to be the RDS and MDS of the WGS reaction catalyzed by TiC(100). Moreover, the very large rate constant (34 orders of magnitude larger than that for the gas-phase reaction) points to a possible effective use of the TiC(001) surface as a catalyst for the WGS reaction. Finally, the transition state of the RDS was only slightly above the energy of the isolated reactants. In this sense, the proper reaction exothermicity would be sufficient to overcome the energy barrier, with a concomitant feedback for the entire process expected. This is important, because it indicates a low energy requirement for the reaction. All of these findings strongly suggest that large TiC particles with (100) facets should be considered as a potential substitute for the Cu-based materials currently used to catalyze the WGS reaction. This is in line with the experimental recommendation to work at temperatures below 300 K, with large (100) facets [80] and low atomic oxygen coverage, to avoid oxycarbide formation [81].

This statement is strongly supported by the comparison between the reaction energy profile predicted for TiC(100) and that reported for other catalytic materials from similar DF calculations [18,47]. Note that these previous studies were carried out using the RPBE [87] functional. Nevertheless, the present tests using RPBE calculations on selected cases found only small adsorption energy deviations, up to 0.1 eV. Moreover, recent DF calculations have shown that energy barriers are less affected by the choice of the exchange-correlation potential than adsorption energies [88] and, in any case, the qualitative results are unaffected [70,71]. This is in line with other studies showing that the relative energies are much less affected by the GGA inherent errors (see Refs. [87, 89–91, and references therein]). Thus, the comparison between different DF studies presented in Fig. 7 is meaningful. The figure clearly shows that $Mo_2C(001)$ surfaces [18], Ti_8C_{12} MetCar and $Ti_{14}C_{13}$ nanocrystal are poor catalyst simply because they bind the different reaction species too strongly. The counterpart is the oxygen-covered metal-terminated $Mo_2C(001)$ surface, which barely binds any of the reaction species, having a reaction energy profile quite similar to that of the gas-phase reaction. The oxygen-covered carbon-terminated $Mo_2C(001)$ surface represents a significant improvement in terms of Sabatier's principle [84], binding the reaction species moderately and with no significant large barriers; however, TiC(001) is closer to the ideal catalyst line, and in fact, the reaction profile is actually similar to that reported for the reaction on Cu(111) [47], which constitutes the active phase of current low-temperature catalysts [12]. This comparison strongly suggests carrying out experiments aimed at corroborating these theoretical predictions.

Before closing this section, we note that it is important to keep in mind that (i) based on the present rate constant estimations, a small, yet nonnegligible fraction (<1%) of the molecules could follow the redox mechanism, leading to a long-term poisoning of the catalyst; (ii) at sufficiently high temperatures, the redox pathway will play a more significant role; and (iii) despite the fact that water dissociation may be accelerated on steps on real extended-surface catalysts, the reaction at these step sites could follow a redox mechanism, thus contributing to possible oxycarbide formation and eventual degradation of the catalytic properties of TiC. The latter observation is based on the results obtained for the nanocrystal, taking this as a suitable model for extended-surface step sites; however, the redox mechanism would be significantly slower on the steps, as indicated by the smaller rate constant on nanocrystal (Table 2). The possible switch to the redox mechanism at high temperatures can be avoided by working at moderate temperatures, which also is important from a production cost standpoint. Note, however, that at the typical working temperatures of 450–520 K corresponding to the Cu-based catalysts, facilitation of the switch between redox and associative mechanisms would be expected, albeit with an increase in the reaction rate.[1] In any case, the use of other TMCs with lower oxygen appetence [38,70,71], such as VC or δ-MoC, could strength the separation of both reaction mechanism, thereby enabling long-term operation.

[1] According to our estimations, associative mechanism would be 100 times faster than redox mechanism in the range of 180–250 °C (450–520 K). In this range, reaction rates would be of the order of 10^5–10^6 for carboxyl formation, and 10^3–10^4 for OH dissociation.

7. Summary and conclusions

We studied the molecular mechanism of the WGS reaction catalyzed by different titanium carbide substrates using suitable models and DF calculations. Three different TiC-based substrates were considered as possible catalysts: the extended TiC(001) surface, the Ti_8C_{12} (MetCar), and the $Ti_{14}C_{13}$ nanocrystal, the latter two being known stable species characterized experimentally [41,42]. Two different molecular reaction mechanism were explored: the commonly assumed redox pathway involving surface atomic oxygen formation and an alternative pathway presuming the existence of a stable carboxyl intermediate found for the WGS reaction on metal surfaces [19,25,47,77,78,80].

A systematic study of the interactions of reactants, intermediates, and products with the different TiC substrates showed that adsorption energies depend not only on the existence of low-coordinated sites, but also on the chemical nature of the atoms involved in the interaction. Despite the fact that the interaction between reaction species and nanoparticles is usually stronger and involves metal sites at the corners, carbon sites at the particle edges and Ti sites at particle facets efficiently compete with the former in many cases. In general, oxygen-connected species tend to adsorb more strongly on the MetCar, whereas carbon-connected species tend to adsorb more strongly on the nanocrystal. Species with a high hydrogen ratio present similar adsorption energies on both the MetCar and the nanocrystal.

Analysis of the calculated energy barriers and of the calculated reaction rate constants predicts that for any of the TiC substrates studied in the present work, the WGS reaction is catalyzed with respect to the gas-phase reaction. But for the $Ti_{14}C_{13}$ and Ti_8C_{12} species, the calculated reaction rate constants indicate that the reaction will not readily occur. In contrast, the reaction above the extended TiC(001) surface appears to be possible and rather efficient. This is accompanied by a change in the preferred mechanism; the redox pathway is clearly favored for the reaction on the MetCar and on the nanocrystal, whereas the carboxyl route clearly dominates on the TiC(001) surface. Also note that the latter mechanism avoids formation of atomic oxygen on the surface thus preventing catalyst deactivation through the formation of oxycarbides. Finally, we point out that, compared with the nanoparticles, the superior catalytic performance of TiC(001) arises from the overly strong interaction of reaction species on the nanoparticles, which results in excessively large energy barriers. Indeed, this provides a nice example of the well-known Sabatier principle [84]. An important corollary of the present work is that the catalytic activity of nanoparticles is not always greater than that of the extended systems; size matters, and monitoring the reactivity through size control seems to be a real possibility, which requires experimental verification.

Finally, we would like to point out that in the commercial catalysts based on supported Cu, as well as those based on, for instance, Au supported on CeO_2, the support likely plays a direct role by accelerating H_2O dissociation, which is the RDS [25]. This is not he case for TiC(001), which is able to spontaneously dissociate H_2O and thus does not require the presence of an active support in the catalyst.

Although the present work considered only TiC-based substrates, it is very likely that a similar behavior holds for the other group IV TMCs as well [36,71]. Moreover, because group V TMCs (or even δ-MoC) have been recently predicted to exhibit greater resistance to atomic oxygen formation on their surfaces [39,70,71], as well as less important oxygen–carbon interactions [38,39,71], it is tempting to suggest that these materials could surpass TiC(001) as catalysts for the WGS reactions, and that they should be considered in model experiments.

Acknowledgments

F.V. thanks the Spanish Ministry of Education and Science (MEC) and Universitat de Barcelona for supporting his predoctoral research. Financial support has been provided by the MEC (grants CTQ2005-08459-CO2-01, UNBA05-33-001) and the Generalitat de Catalunya (2005SGR00697, 2005 PEIR 0051/69). Generous allocation of computational time on the MARENOSTRUM supercomputer of the Barcelona Supercomputing Center is gratefully acknowledged.

References

[1] K. Klier, C.W. Young, J.G. Nunan, Ind. Eng. Chem. Fund. 25 (1986) 36.
[2] D.S. Newsome, Catal. Rev. Sci. Eng. 21 (1980) 275.
[3] M.V. Twigg, Catalyst Handbook, Wolfe, London, 1989.
[4] R.D. Cortright, R.R. Davda, J.A. Dumesic, Nature 418 (2002) 964.
[5] Y. Liu, Q. Fu, M. Flytzani-Stephanopoulos, Catal. Today 93–95 (2004) 241.
[6] D.J. Suh, C. Kwak, J.H. Kim, S.M. Kwon, T.J. Park, J. Power Sources 142 (2005) 70.
[7] C. Song, Catal. Today 77 (2002) 17.
[8] R. Burch, Phys. Chem. Chem. Phys. 8 (2006) 5483.
[9] Q. Fu, H. Saltsburg, M. Flytzani-Stephanopoulos, Science 301 (2003) 935.
[10] G. Germani, Y. Schuurman, AIChE J. 52 (2006) 1806.
[11] C. Rhodes, G.J. Hutchings, A.M. Ward, Catal. Today 23 (1995) 43.
[12] H. Bohlbro, M.H. Jørgensen, Chem. Eng. World 5 (1970) 46.
[13] N. Schumacher, A. Boisen, S. Dahl, A.A. Gokhale, S. Kandoi, L.C. Grabow, J.A. Dumesic, M. Mavrikakis, I. Chorkendorff, J. Catal. 229 (2005) 265.
[14] V. Idakiev, T. Tabakova, Z.Y. Yuan, B.L. Su, Appl. Catal. A Gen. 270 (2004) 135.
[15] X. Wang, J.A. Rodríguez, J.C. Hanson, D. Gamarra, A. Martinez-Arias, M. Fernandez-Garcia, J. Phys. Chem. B 109 (2005) 19595.
[16] H. Sakurai, T. Akita, S. Tsubota, M. Kiuchi, M. Haruta, Appl. Catal. A Gen. 291 (2005) 197.
[17] X. Wang, J.A. Rodríguez, J.C. Hanson, M. Perez, J. Evans, J. Chem. Phys. 123 (2005) 221101.
[18] P. Liu, J.A. Rodriguez, J. Chem. Phys. 126 (2007) 164705.
[19] J.A. Rodriguez, P. Liu, J. Hrbek, J. Evans, M. Perez, Angew. Chem. Int. Ed. 46 (2007) 1329.
[20] W. Deng, M. Flytzani-Stephanopoulos, Angew. Chem. Int. Ed. 45 (2006) 2285.
[21] D. Tibiletti, A. Amieiro-Fonseca, R. Burch, Y. Chen, J.M. Fisher, A. Goguet, C. Hardacre, P. Hu, D. Thompsett, J. Phys. Chem. B 109 (2005) 22553.
[22] Z.P. Liu, S.J. Jenkins, D.A. King, Phys. Rev. Lett. 94 (2005) 196102.
[23] S. Ricote, G. Jacobs, M. Milling, Y.Y. Ji, P.M. Patterson, B.H. Davis, Appl. Catal. A Gen. 303 (2006) 35.
[24] T. Bunluesin, R.J. Gorte, G.W. Graham, Appl. Catal. Environ. 15 (1998) 107.
[25] J.A. Rodriguez, S. Ma, P. Liu, J. Hbrek, J. Evans, M. Perez, Science 318 (2007) 1757.
[26] C.H. Kim, L.T. Thompson, J. Catal. 230 (2005) 66.
[27] X.S. Liu, W. Ruettinger, A.M. Xu, R. Farrauto, Appl. Catal. B 56 (2005) 69.
[28] R.B. Levy, M. Boudart, Science 181 (1973) 547.
[29] H.H. Hwu, J.G. Chen, Chem. Rev. 105 (2005) 185.
[30] S.T. Oyama, Catal. Today 15 (1992) 179.
[31] D.J. Moon, J.W. Ryu, Catal. Lett. 92 (2004) 17.
[32] J. Patt, D.J. Moon, C. Phillips, L. Thompson, Catal. Lett. 65 (2000) 193.
[33] P. Liu, J.A. Rodriguez, J. Phys. Chem. B 110 (2006) 19418.
[34] P. Liu, J.A. Rodriguez, J. Chem. Phys. 119 (2004) 10895.
[35] P. Liu, J.A. Rodriguez, J.T. Muckerman, J. Chem. Phys. 121 (2004) 10321.
[36] F. Viñes, C. Sousa, P. Liu, J.A. Rodriguez, F. Illas, J. Chem. Phys. 122 (2005) 174709.
[37] J.G. Chen, C.M. Kim, B. Frühberger, B.D. DeVries, M.S. Trouvelle, Surf. Sci. 312 (1994) 145.
[38] F. Viñes, C. Sousa, F. Illas, P. Liu, J.A. Rodriguez, J. Phys. Chem. C 111 (2007) 1307.
[39] J.A. Rodriguez, P. Liu, J. Gomes, K. Nakamura, F. Viñes, C. Sousa, F. Illas, Phys. Rev. B 72 (2005) 075427.
[40] J.A. Rodriguez, P. Liu, J. Dvorak, T. Jirsak, J. Gomes, Y. Takahashi, K. Nakamura, Phys. Rev. B 69 (2004) 115414.
[41] B.C. Guo, K.P. Kerns, A.W. Castleman Jr., Science 225 (1992) 1411.
[42] J.S. Pilgrim, M.A. Ducan, J. Am. Chem. Soc. 115 (1993) 9724.
[43] J.M. Lightstone, J.M. Patterson, P. Liu, W.G. White, J. Phys. Chem. A 110 (2006) 3505.
[44] P. Liu, J.M. Lightstone, J.M. Patterson, J.A. Rodriguez, J.T. Muckerman, M.G. White, J. Phys. Chem. B 110 (2006) 7449.
[45] P. Liu, J.A. Rodriguez, J.T. Muckerman, J. Phys. Chem. B 108 (2004) 18796.
[46] H. Tominaga, M. Nagai, J. Phys. Chem. B 109 (2005) 20415.
[47] A.A. Gokhale, J.A. Dumesic, M. Mavrikakis, J. Am. Chem. Soc. 130 (2008) 1402.
[48] J.R. Kitchin, J.K. Nørskov, M.A. Barteau, J.G. Chen, Catal. Today 105 (2005) 66.

[49] P. Liu, J.A. Rodriguez, J. Chem. Phys. 120 (2004) 5414.
[50] P. Liu, J.A. Rodriguez, H. Hou, J.T. Muckerman, J. Chem. Phys. 118 (2003) 7737.
[51] S.V. Didziulis, P. Frantz, L.C. Fernandez-Torres, R.B. Guenard, O. El-bjeirami, S.S. Perry, J. Phys. Chem. B 105 (2001) 5196.
[52] J.P. Perdew, Y. Wang, Phys. Rev. B 45 (1992) 13244.
[53] P.E. Blöchl, Phys. Rev. B 50 (1994) 17953.
[54] G. Kresse, J. Hafner, Phys. Rev. B 47 (1993) 558.
[55] G. Kresse, J. Furthmüller, Comput. Mater. Sci. 6 (1996) 15.
[56] G. Kresse, J. Furthmüller, Phys. Rev. B 54 (1996) 11169.
[57] F. Viñes, A. Desikusumastuti, T. Staudt, A. Görling, J. Libuda, K.M. Neyman, J. Phys. Chem. C (2008), DOI: 10.1021/jp804315c.
[58] A. Roldán, F. Viñes, F. Illas, J.M. Ricart, K.M. Neyman, Theor. Chem. Acc. 120 (2008) 565.
[59] F. Viñes, F. Illas, K.M. Neyman, J. Phys. Chem. A 112 (2008) 8911.
[60] L.S. Wang, H. Cheng, Phys. Rev. Lett. 78 (1997) 2983.
[61] S. Li, H. Wu, L.S. Wang, J. Am. Chem. Soc. 119 (1997) 7417.
[62] J.O. Joswig, M. Springborg, G. Seifert, Phys. Chem. Chem. Phys. 3 (2001) 5130.
[63] I. Dance, J. Chem. Soc. Chem. Commun. (1992) 1779.
[64] I. Dance, J. Am. Chem. Soc. 118 (1996) 6309.
[65] N. Blessing, S. Burkart, G. Ganteför, Eur. Phys. J. D 17 (2001) 37.
[66] G.K. Gueorguiev, J.M. Pacheco, Phys. Rev. Lett. 88 (2002) 115504.
[67] P. Liu, J.A. Rodriguez, H. Hou, J.T. Muckerman, J. Chem. Phys. 118 (2003) 7737.
[68] K. Henkelman, H. Jonson, J. Chem. Phys. 117 (2000) 303.
[69] G. Henkelman, B.P. Uberuaga, H. Jonsson, J. Chem. Phys. 113 (2000) 9901.
[70] Y.F. Zhang, F. Viñes, Y.J. Xu, Y. Li, J.Q. Li, F. Illas, J. Phys. Chem. B 110 (2006) 15454.
[71] F. Viñes, C. Sousa, F. Illas, P. Liu, J.A. Rodriguez, J. Phys. Chem. C 111 (2007) 16982.
[72] K.J. Laidler, Chemical Kinetics, third ed., Harper Collins, New York, 1987.
[73] L.C. Grabow, A.A. Gokhale, S.T. Evans, J.A. Dumesic, M. Mavrikakis, J. Phys. Chem. C 112 (2008) 4608.
[74] C.V. Ovensen, B.S. Clausen, J. Schiøtz, P. Stoltze, H. Topsøe, J.K. Nørskov, J. Catal. 168 (1997) 133.
[75] C.V. Ovensen, P. Stoltze, J.K. Nørskov, C.T. Campbell, J. Catal. 134 (1992) 445.
[76] C. Wheeler, A. Jhalani, E.J. Klein, S. Tummala, L.D. Schmidt, J. Catal. 223 (2004) 191.
[77] T. Shido, Y. Iwasawa, J. Catal. 141 (1993) 71.
[78] J. Nakamura, J.M. Campbell, C.T. Campbell, J. Chem. Soc. Faraday Trans. 86 (1990) 2725.
[79] N. Liu, S.A. Rykov, J.G. Chen, Surf. Sci. 487 (2001) 107.
[80] S. Nakamura, Y. Takahashi, A. Ivanova, K. Nakamura, in preparation.
[81] J.A. Rodríguez, P. Liu, J. Dvorak, T. Jirsak, J. Gomes, Y. Takahashi, K. Nakamura, J. Chem. Phys. 121 (2004) 465.
[82] Y. Zhao, A.C. Dillon, Y.H. Kim, M.J. Heben, S.B. Zhang, Chem. Phys. Lett. 425 (2006) 273.
[83] N. Akman, E. Durgun, T. Yildirim, S. Ciraci, J. Phys. Condens. Matter 18 (2006) 9509.
[84] P. Sabatier, La Catalyse in Chemie Onargique, Libraire Polytechnique, Paris, 1913.
[85] S. Aido, Y. Takahashi, F. Viñes, P. Liu, F. Illas, J.A. Rodriguez, K. Nakamura, in preparation.
[86] S. González, D. Loffreda, P. Sautet, F. Illas, J. Phys. Chem. C 111 (2007) 11376.
[87] B. Hammer, L.B. Hansen, J.K. Nørskov, Phys. Rev. B 59 (1999) 7413.
[88] A. Roldán, S. Gonzalez, J.M. Ricart, F. Illas, submitted for publication.
[89] C.H. Christensen, J.K. Nørskov, J. Chem. Phys. 128 (2008) 182503.
[90] K. Honkala, A. Hellman, I.N. Remediakis, A. Logadottir, A. Carlsson, S. Dahl, C.H. Christensen, J.K. Nørskov, Science 307 (2005) 555.
[91] P. Strasser, Q. Fan, M. Devenney, W.H. Weinberg, P. Liu, J.K. Nørskov, J. Phys. Chem. B 107 (2003) 11013.